Master's Thesis

Patterned ZnO on PDMS with MXene Quantum Dot (MQD) for Triboelectric Nano-generators

Suhee Kim

Department of Chemical Engineering

Graduate School of UNIST

2020

Patterned ZnO on PDMS with MXene Quantum Dot (MQD) for Triboelectric Nano-generators

Suhee Kim

Department of Chemical Engineering

Graduate School of UNIST

Patterned ZnO on PDMS with MXene Quantum Dot (MQD) for Triboelectric Nano-generators

A thesis/dissertation
submitted to the Graduate School of UNIST
in partial fulfillment of the
requirements for the degree of
Master of Science

Suhee Kim

06/11/2020

Approved by

Advisor
Ji-Hyun Jang

Patterned ZnO on PDMS with MXene Quantum Dot(MQD) for Triboelectric Nanogenerators

Suhee Kim

This certifies that the thesis/dissertation of Suhee Kim is approved.

06.11.2020 of submission

signature

Advisor: Ji-Hyun Jang

signature

Hyun-Kon Song

signature

Young-Bin Park

Abstract

Triboelectric nano-generators (TENG) is an emerging technology for the development of the IoT (Internet of Thing) and has been a popular research topic in recent years. This thesis covered nanopattern TENG with high power generation performance through structural / chemical improvements. Nanopatterned polydimethylsiloxane (PDMS) based on MXene Quantum Dot (MQD) coated ZnO array were used as active material. Friction was applied at short intervals with a force of 4.8 kgf, and a current of 300 nA / cm2 was observed in the nano-patterned PDMS-based TENG device. This is based on the structure of nanopatterned PDMS and surface chemistry through MQD, and it was confirmed that MQD enhanced the electrostatic phenomenon by maximizing the effect of the negative layer.

Contents

List of Figures

List of Table

Chapter 1. Introduction of Triboelectric Nanogenerators (TENG)

1.1 Energy Harvesting

Over the past decades, there is a growing need and interest in energy harvesting technology that harvests energy that is thrown away by soaring energy consumption and the depletion of natural resources into electrical energy. Energy harvesting technology was introduced for the first time in 1954 when the U.S. Bell Labs researched solar cells that convert sunlight into energy. It is a form that is converted into electric current and stored for later use. Typical energy harvesting technologies can be broadly classified into thermoelectric[1], photoelectric[2], piezoelectric, and wind[3](Fig. 1). Although it is best known in the field of solar cells, the recent increase in the number of Internet of Things (IoT) sensors has led to an increasing number of attempts to make equipment self-supply without battery replacement. Among various energy harvesting methods, the triboelectric nano-generator (TENG) has an important advantage in that it is environmentally friendly, high efficiency, low cost, and not significantly affected by the operating environment unlike other energy harvesting devices (solar, thermoelectric, wind, etc.)[4].

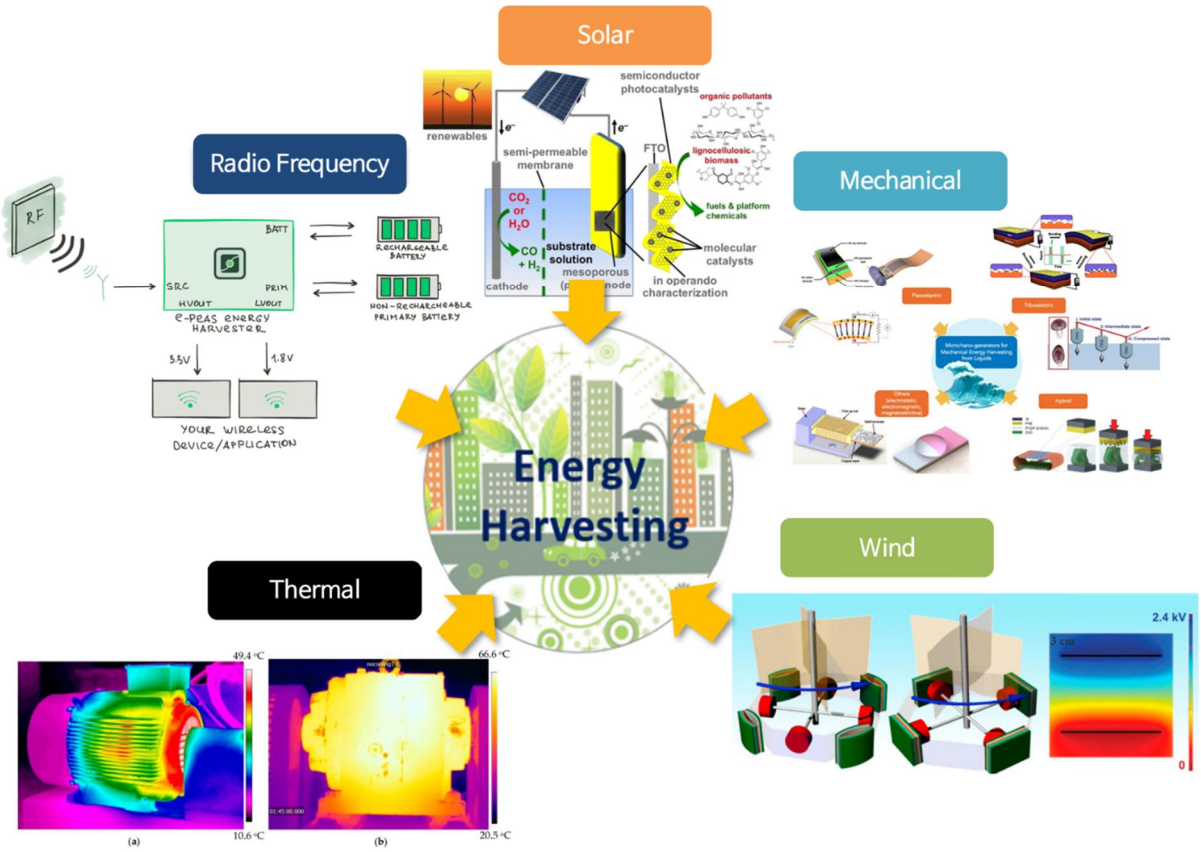

Figure 1. Kind of Energy Harvesting

1.2 Triboelectric Nanogenerator (TENG)

The triboelectric generator, first developed by the Wang Group in 2012[5], has the advantage of being made of high efficiency, simple structure, and inexpensive material. TENG is based on the principle that electricity is produced by repetition of charging and electrostatic induction phenomena caused by the contact of different objects.

As shown in Figure 2, when two materials with different triboelectric series are touched, the material with a relatively negative triboelectric series is charged with (-) and the other material is charged with (+). In the charged state, the electrodes are fixed on the friction material, connected by wires, and when the two materials begin to separate, electrons move to achieve electrical balance. With this principle, the triboelectric generator converts mechanical kinetic energy into electrical energy.

The TENG generator converts energy in four operation methods depending on the polarization change direction and electrode configuration, and is applied to appropriate applications. (Fig. 4). In addition to aspects of the energy conversion method, numerous studies have been conducted on improving TENG performance. It has been extensively investigated for the modification of charged materials, the effects of contact, and environmental changes (Fig. 5).

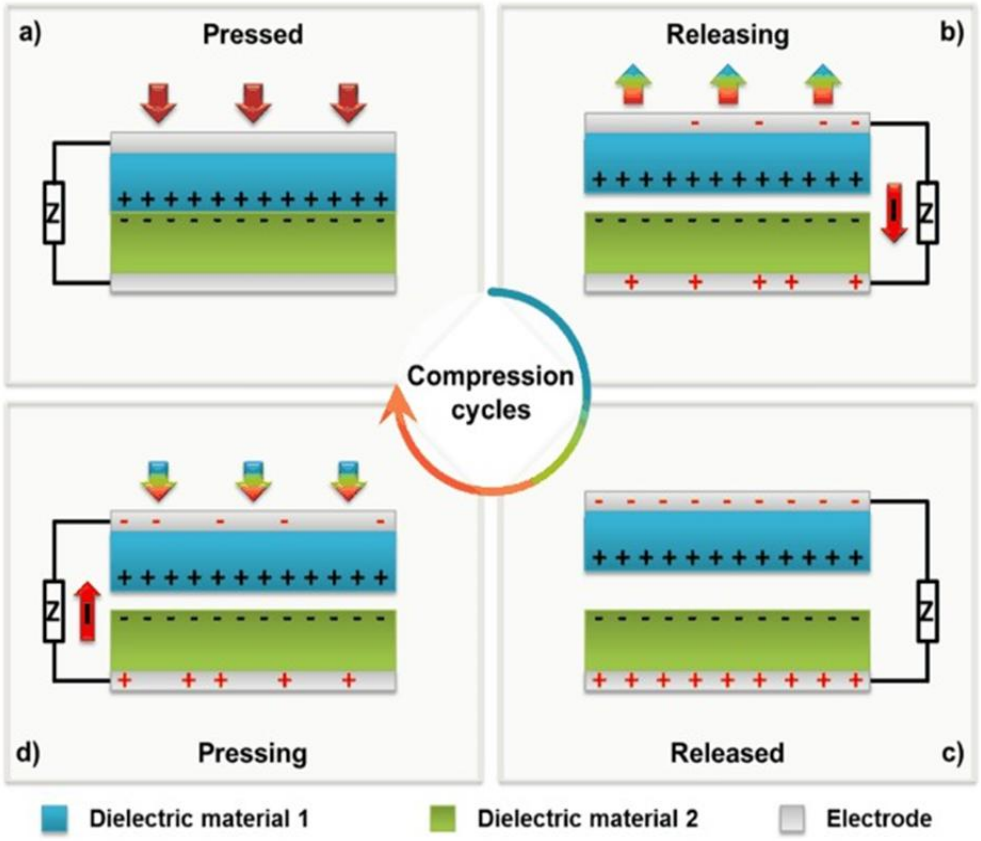

Figure 2. The principle of Triboelectric nanogenerators (TENG)[6]

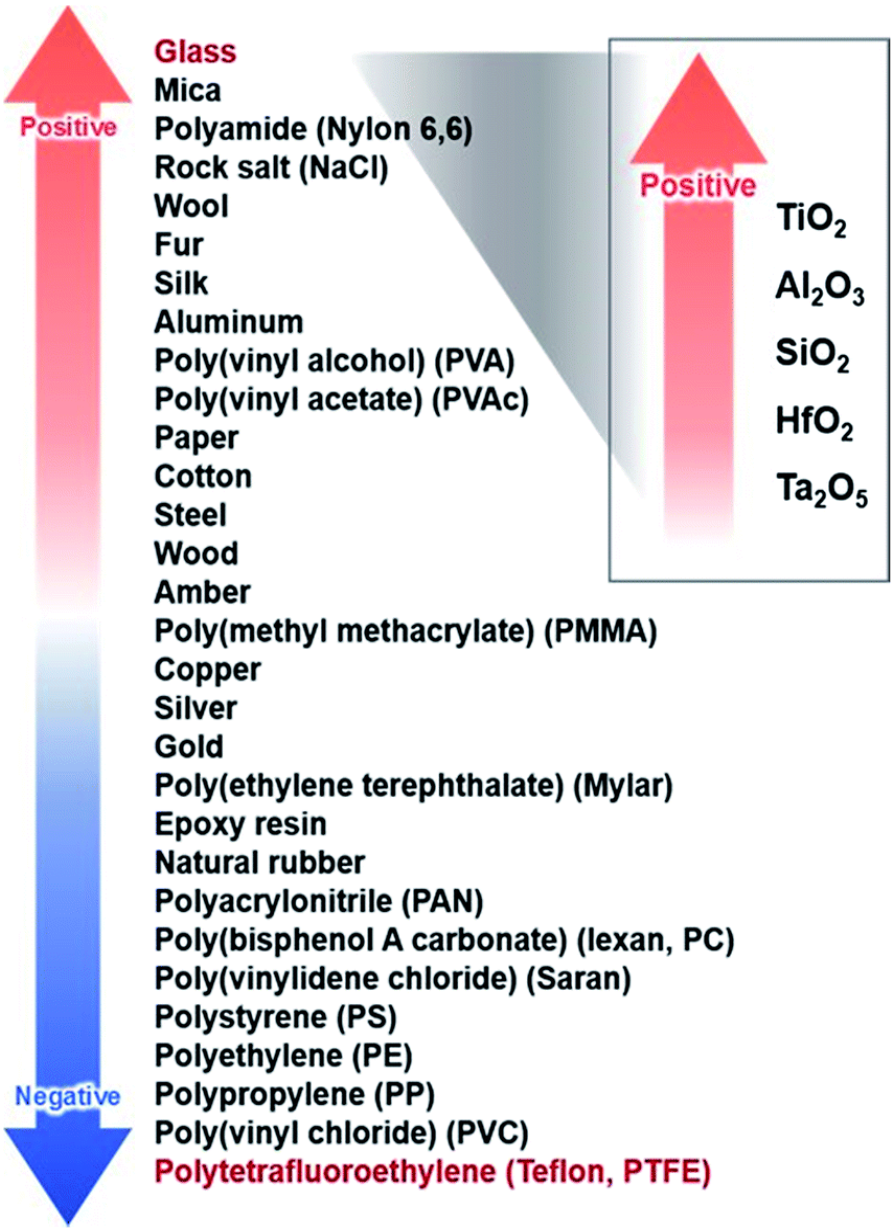

Figure 3. Triboelectric series[7]

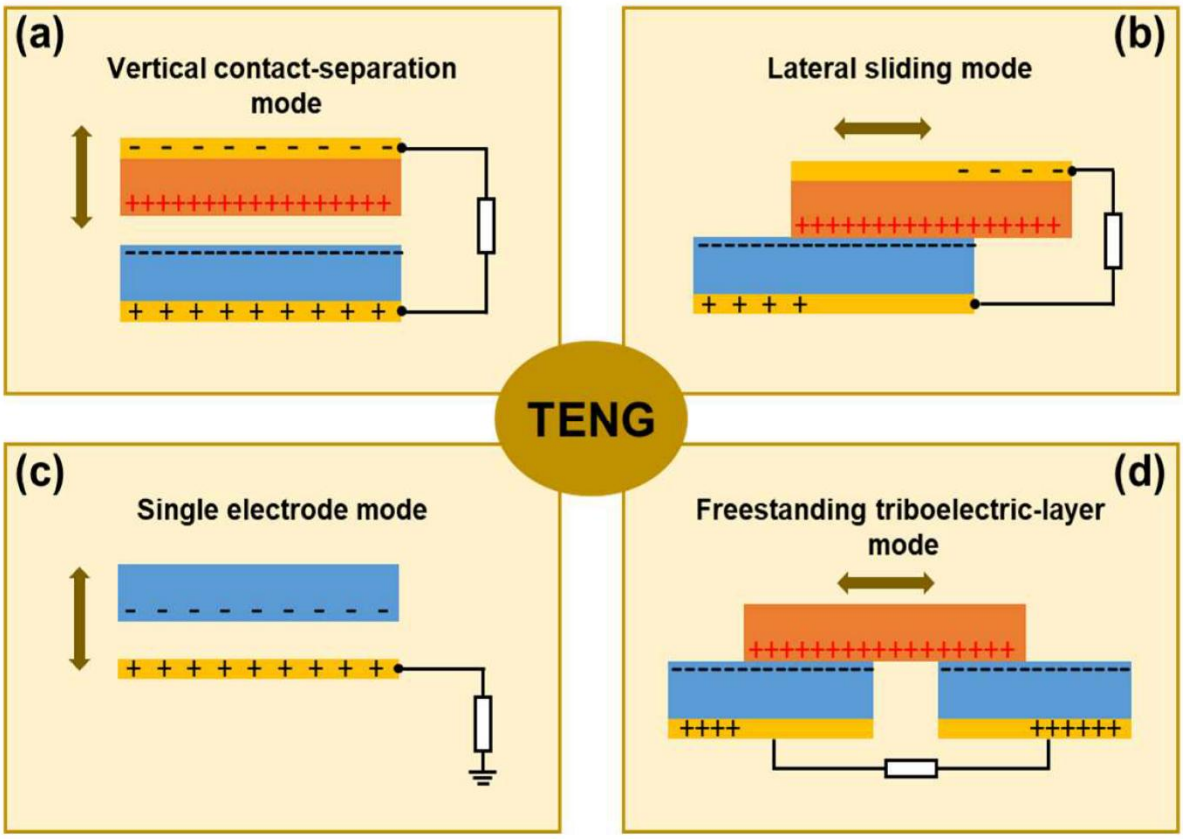

Figure 4. 4 different operation mode of the TENG[8]

Chapter 2. MXene Quantum Dot(MQD) on Patterned PDMS with ZnO for Triboelectric Nanogenerators

2.1 Introduction

TENG can be driven by simple structure and simple packaging, and has high output energy density. In addition, TENG is made of flexible and transparent materials, so it can be applied to various places. Although TENG has been intensively studied, the problems related to energy loss in the power generation process remain a big challenge to overcome.

Among the various types of triboelectric materials, poly(dimethyl siloxane) (PDMS) is a kind of negative friction layer candidate due to its high electronegativity, good transparency, flexibility and good mechanical strength. In addition, ZnO is a semiconductor material with a wide band gap of 3.37 eV[9], and is suitable as a TENG material that can be applied in various ways with high optical propertie and human-friendly stabiliy. However, the output performance of ZnO-based TENG is relatively low, so it is necessary to improve the performance.

Here, we grow ZnO on nanopattern PDMS to increase power production. The ZnO nanostructure on the patterned PDMS can be used as an excellent material because it can improve the performance of TENG as an important strategy to reduce energy loss by increasing the surface area of the substrate. MXene quantum dot (MQD) is a very negatively charged material that helps effectively generate current by increasing the gap between the triboelectric series and the opposite pole.

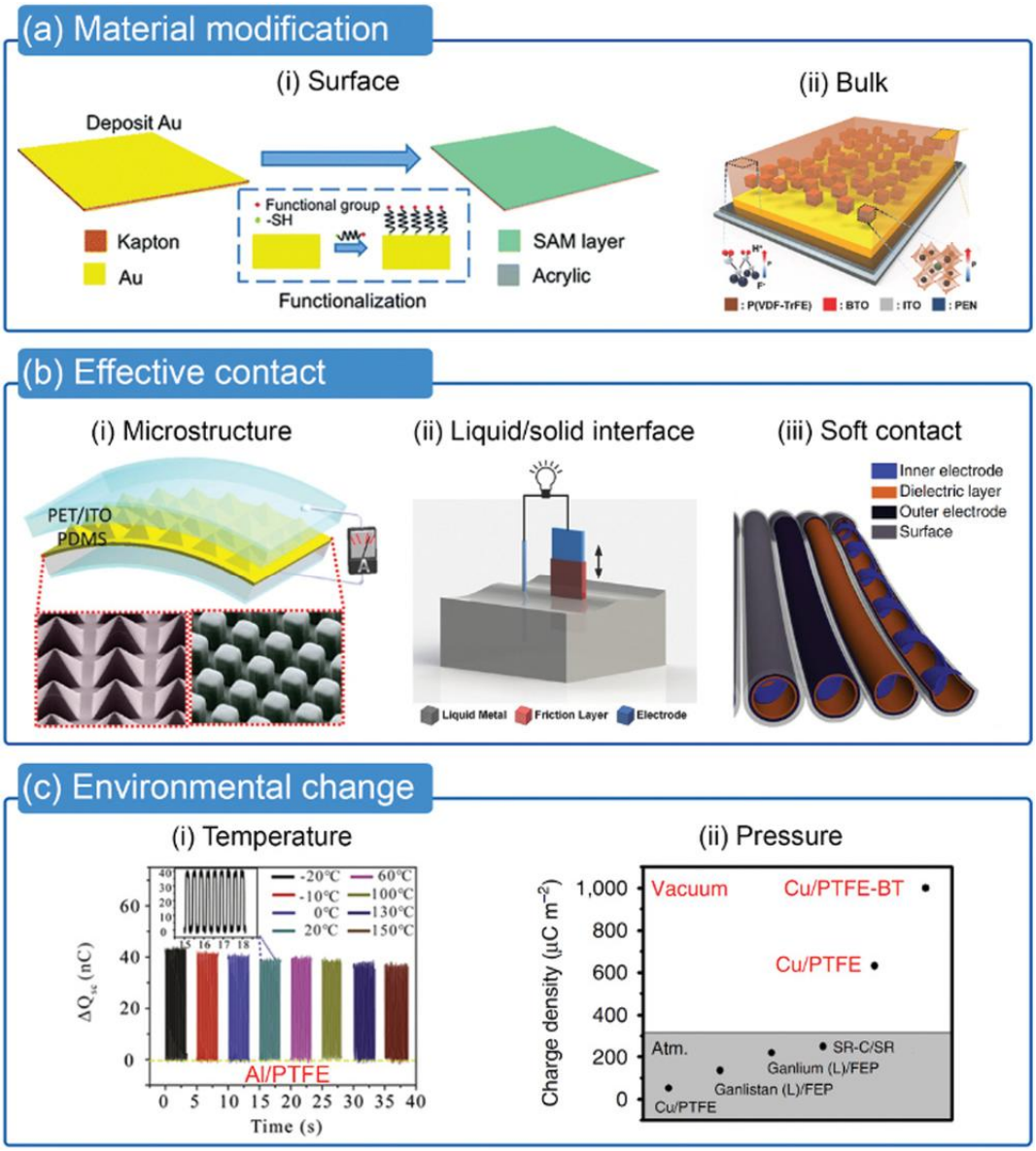

Figure 5. Strategies for improving performance[10]

2.1.1 MXene(Ti3C2)

MXenes are family of 2D transition metal carbides, nitrides or carbonitrides. These are formed by selective etching MAX compounds. The chemical compositions of MAX phases are traditionally known Mn+1AXn, where n=1,2,3, M is an early transition metal(Ti, Sc, Zr, Hf, V, Nb, Ta, Cr, Mo), A is an elements from group periodic 13-14(Al, Ga, In, Tl, Si, Ge, Sn, Pb, P, As, Bi, S, Te), and X is carbon or nitrogen[11] (Fig. 6). For synthesis MXene, A group is removed usually by using acid treatment. The resulting material called MXene and general formula is Mn+1XnTx, T is surface termination (-OH, =O, -F).

The result of MXene varies depending on the etching process[12]. When HF acid is used, only Al is removed to create an accordion-type multi-layered structure. When the intercalation salt such as HCl acid and LiF are added together, Li+ ions enter the place where Al is removed, and delamination proceeds together, and MXene in the form of a single layer is produced. In addition, in the case of multilayered MXene, it can be transformed into a single layer type if additional energy is applied. MXenes offer an attractive combination of high electronic conductivity, hydrophilicity, and chemical stability present in 2D sheet type. Due to these advantages, MXene is attracting attention as a promising candidate in electromagnetic interference shielding, chemical sensing, wireless communication, and energy storage[13-15].

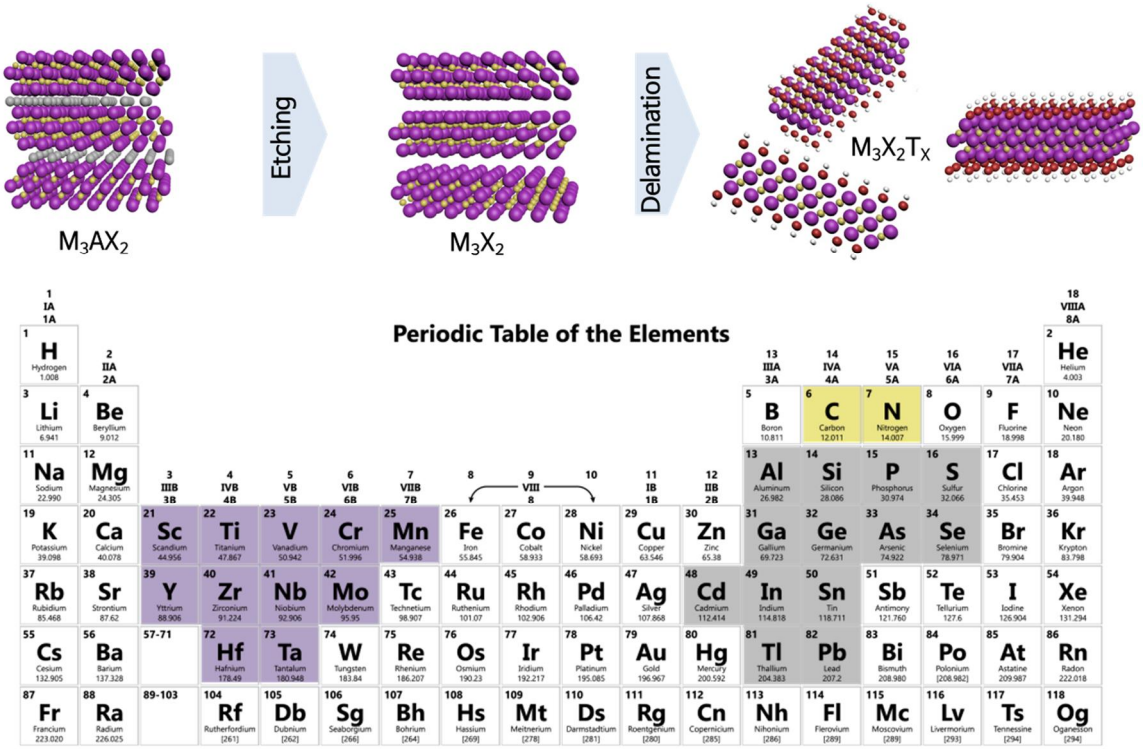

Figure 6. Top-down synthesis of MXene from MAX and periodic table

2.2 Experimental

2.2.1 Synthesis of MXene

Single layered Ti3C2Tx was synthesized through delamination the MAX(Ti3AlC2) phase with HCl/LiF. Briefly, 20ml of 9mol HCl and 1g of LiF powder were mixed in plastic vial for 10min with Teflon stirring bar. And 1g of MAX powder are carefully added to avoid initial overheating of solution for 10-15 minuites. Then the mixture was held oil bath at 35°C, 500rpm for 24 hours, after which mixture was washed with 1000ml of DI water to the product reached a pH 6 by using centrifuge process (3500 rpm, 5 min for each cycle). After that, delamination was conducted by batch sonication.

2.2.2 Synthesis of MXene Quantum Dot (MQD)

Briefly, obtained MXene was dried on vacuum oven at 60°C. 100mg of Ti3C2(MXene) were re-dispersed in 40 mL of Dimethyl Sulfoxide (DMSO) for 12h with stirring. and ultrasonication was conducted to make MXene nanoparticles (NPs). After 12 hours, MXene intercalated with DMSO was separated from DMSO using a PTFE filter, and solvent exchage with water using ethanol and water. Ultrasonication was conducted to make MXenes into MXene nanoparticles (NPs). For MQD synthesis, 0.2 ml PEI (polyethylenimine, MW =25k) was added to 2 ml of MXene NPs solution and 40 ml of water mixture and stirred for 2 hours. The solution was transferred to a 100ml Teflon-lined stainless steel autoclave. And the hydrothermal reaction was performed at 120°C for 4 h. The resulting black solution was filtered through a 0.22μm cellulose acetate(CA) membrane filter, and a clear filtered solution was separated. Eventually, the solution was further dialyzed in a dialysis bag (retained molecular weight: 1 kDa) for 3 days to obtain the Ti3C2 QDs (MQD).

2.2.3 Synthesis of Patterned PDMS

Polydimethylsiloxane prepolymer and curing agent with the ratio of 10:1 were used for nano-patterned PDMS composite. The polymer mixture was poured on a patterned mold and it was left in the oven until curing was finished.

2.2.4 Preparation MQD on Patterned PDMS with ZnO

The hydrothermal method was used to synthesize ZnO on patterned PDMS. First, Zn seeds were deposited uniformly by a DC sputtering system. To grow ZnO around seeds, patterned PDMS treated

with DC sputter were floated on Zn (NO3)2 ▪ 4H2O and C6H12N4 solutions preheated at 100 °C. The PDMS substrate was reacted at 100°C for 150 minutes, and washed with DI water and Ethanol.

2.2.5 Characterization

The morphology of the material was observed by SEM (S-4800, Hitachi) and TEM(JEM-2100, JEOL, 200 kV). The phase and crystalline structure of the material was analyzed using XRD (D/Max 2000, Rigaku). XPS was performed using a surface analysis system (K-alpha, Thermo Fisher). Surface area was obtained using nitrogen physisorption analyzer (ASAP2420, Micromeritics instruments).

2.3 Results and Discussion

MXene sheets have been successfully synthesized by using 1g of LiF and 9M HCl solution according to literature[12]. Figure 7, shows a SEM image of the MAX and MXene. Before etching process, MAX presents tightly stacked flake. After LiF-HCl selective etching process MXene show 2D sheet type shape. Figure 8.(a) show X-ray diffraction(XRD) pattern of the pristine MAX (Ti3AlC2) and MXene (Ti3C2Tx). Ti3AlC2 displayed characteristic intense peaks at 2θ = 9.54°, 19.17°, 33.99°, 38.99° and 40.89° corresponding to the planes (002), (004), (101), (104) and (105), respectively. In the MXene pattern, the most intense peak of Ti3AlC2 located at (104) was completely absent due to the etching process. Also, the (002) peak of MXene became broadened and shifted to 5.82°. At the same time, two new peaks emerged at 2θ = 8.24° (006), and 28.24° (008). The Raman spectroscopy (Fig. 8.(b)) show exist of Ti on wavenumber range of 100-800cm-1 and C on wave number of 500-700cm-1. The BET measurement was performed to confirm the increase in surface area (1.2 m2/g to 18.8 m2/g) resulting from the change in the form of a 2D sheet by etching.

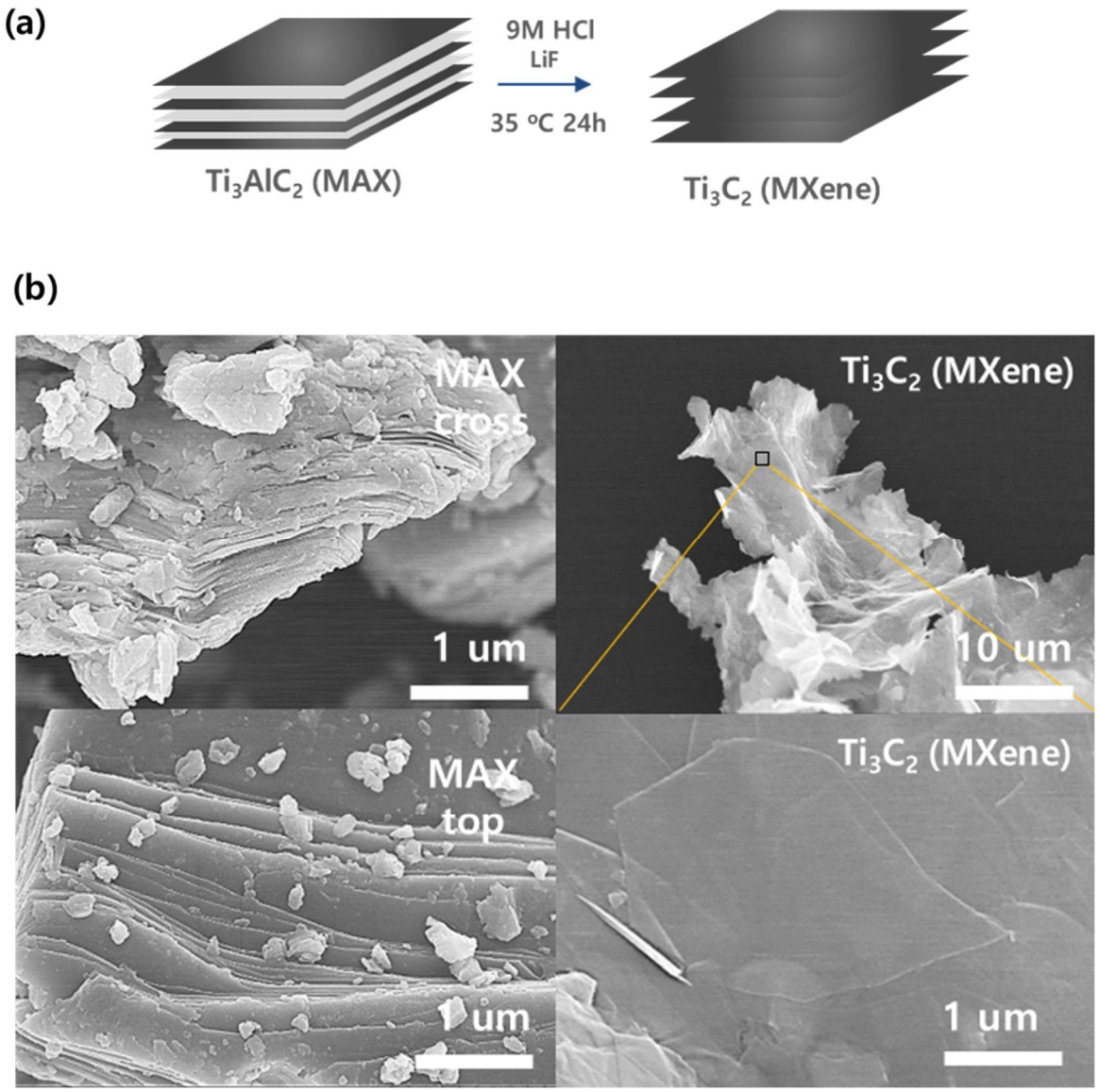

Figure 7. (a) MXene etching process, (b) SEM image of Ti_3AlC_2 (MAX) and Ti_3C_2 (MXene) sheet

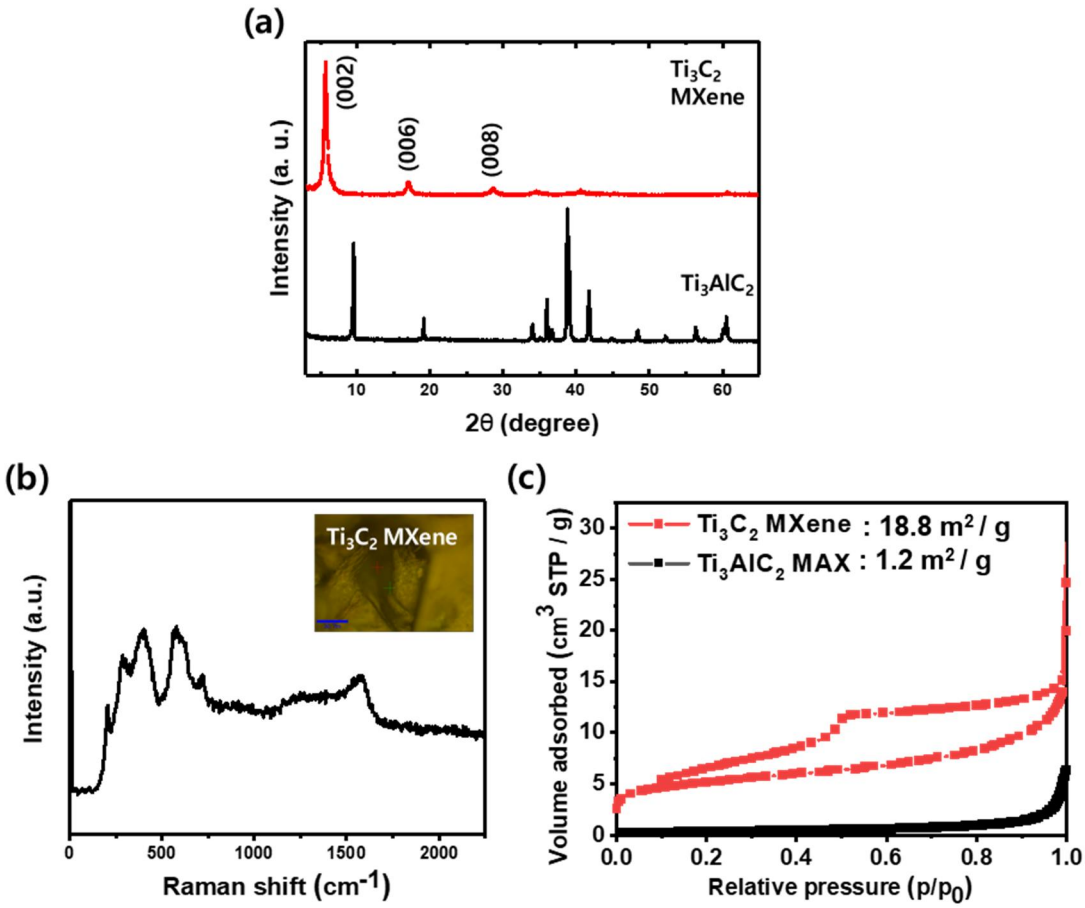

Figure 8. (a) XRD (b) Raman (c) BET spectra of MAX and Ti_3C_2 (MXene)

As shown in Figure 9.(a), MQD was produced in a top-down method using MXene NPs and PEI. In photoluminescence measurements, MQDs show emission bands in the 450-600 nm region centered on 350 nm, which can be seen as evidence of quantum dot formation. The graph on the left in Figure 9.(b) demonstrates that the PL emission band represented by the MQD PEI solution is not the effect of PEI. In UV light, the solution with only PEI shows a brighter luminescence, but shows very low intensity when measuring PL, showing that the luminescence in the MQD PEI solution originates from MQD. The graph on the right in Figure 9.(b) shows the PL intensity according to the molecular weight of PEI. Since the intensity is related to the indirect yield of MQD, we used MQD synthesized using PEI with a molecular weight of 25k.

The composition of MQD was investigated by X-ray photoelectron spectroscopy (XPS). As shown in Table 1, Atomic percentage shows the presence of Ti, C and O, the composition of MXene. Also, we need to pay attention to the graph in Figure 10.(d). The presence of Ti-C sp1 and Ti-C sp3 peaks is another evidence that MXene is split into MXene quantum dots without additional reactions such as oxidation while maintaining its stable structure.

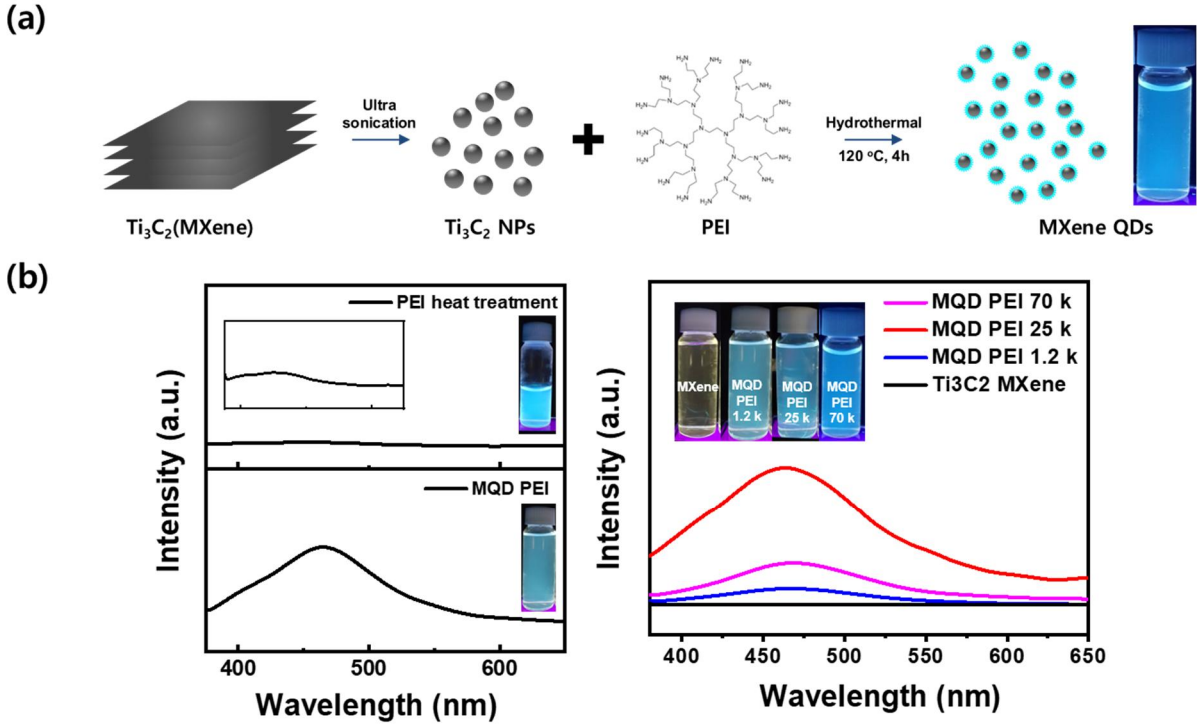

Figure 9. (a) Synthesis process of MQDs, (b) Photoluminescence of MQD

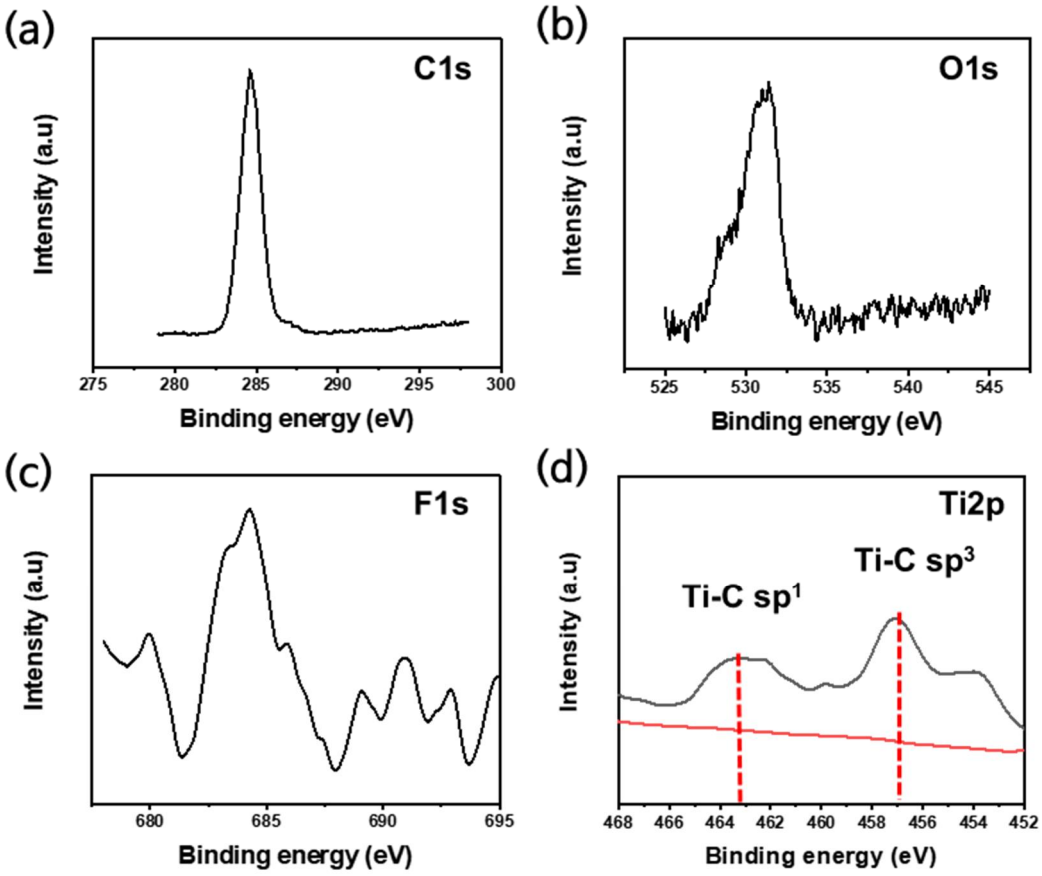

Figure 10. XPS spectra of MQD

Element	Atomic %
C1s	63.7
O1s	8.08
Ti2p	1.39

Table 1. Component atomic percentage of MQD by XPS

Figure 11. show the fabrication of patterned PDMS and vertically aligned ZnO on patterned PDMS. The nano Patterned PDMS was simply produced by pouring and curing PDMS into a mold with a patterned pattern. The SEM image (Fig. 11(b)) shows that the PDMS with the pattern formed was synthesized. ZnO was grown on a patterned PDMS through a hydrothermal method. For vertically aligned ZnO, ZnO seeds were first laid through DC sputtering and heat treated in solution (Fig. 12). The hydrothermal-grown ZnO layer crystallinity was examined using a XRD (Fig. 13). The XRD results show that ZnO is vertically aligned on the PDMS by seeing only the (002) phase of the ZnO peak. In Figure 11.(b), the EDS elemental maps demonstrated that ZnO layer are uniformly distributed on the patterned PDMS anode.

MQD was sprayed on the PDMS with uniformly grown ZnO for the negative layer effect. The form of MQD sprayed on ZnO was confirmed by TEM image of Figure 14. The completed MQD/ZnO/PDMS electrode (3 x 3 cm2) was assembled with PET/ITO electrode for measurement. (Fig. 15).

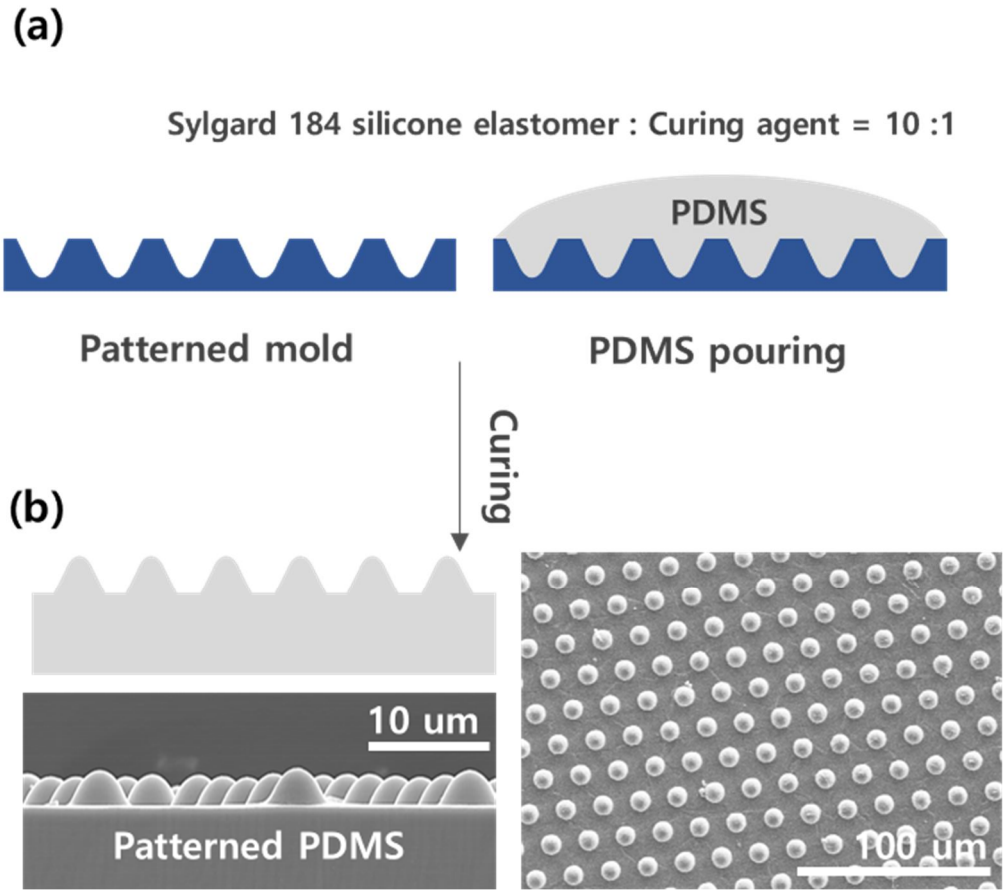

Figure 11. Fabrication of patterned PDMS

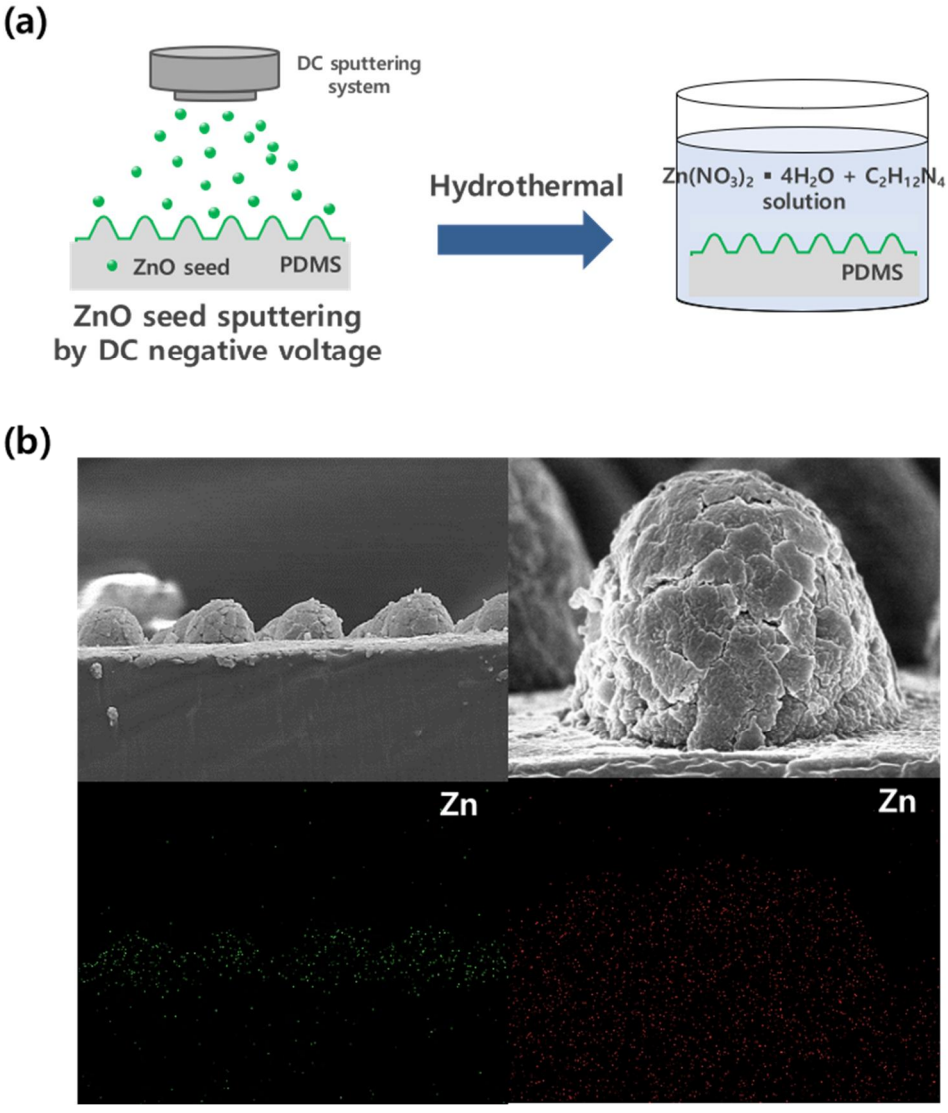

Figure 12. (a) Process of ZnO array on PDMS, (b) SEM, EDS image of ZnO on PDMS

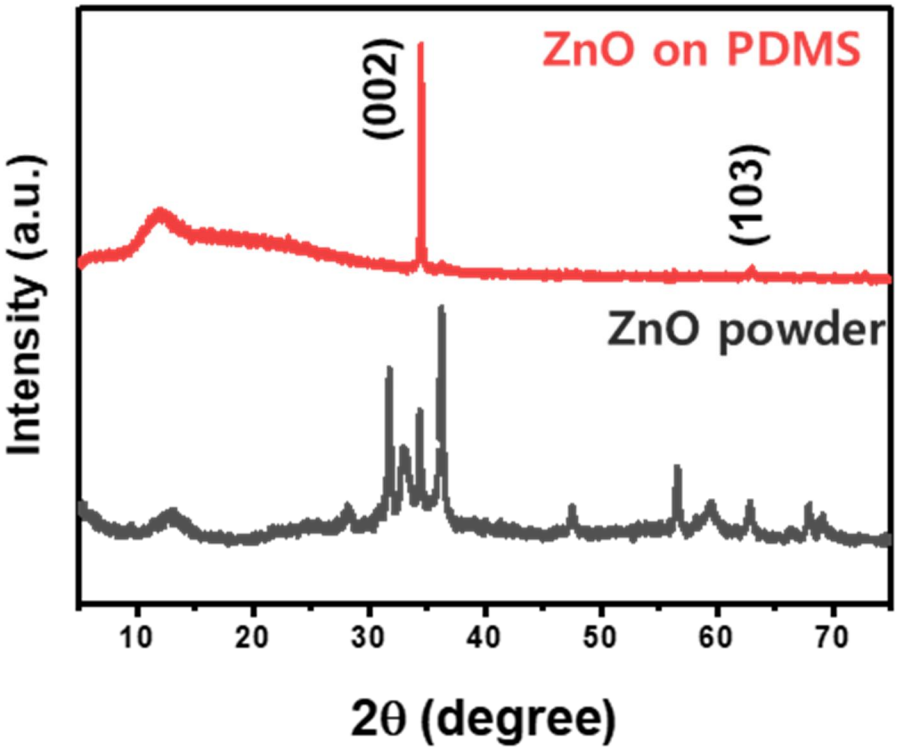

Figure 13. XRD spectra of ZnO on PDMS

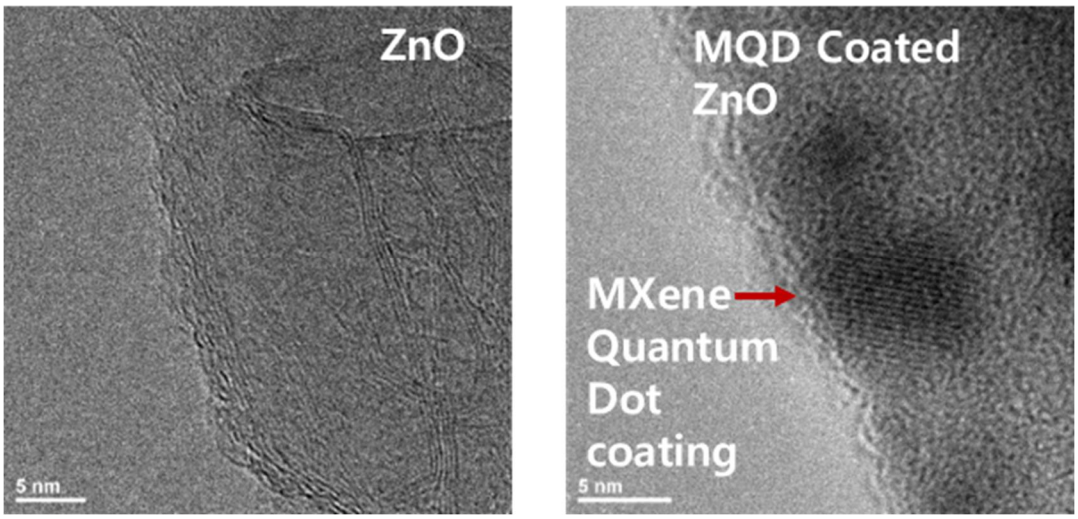

Figure 14. TEM image of MQD coated ZnO

The designed electrode was assembled for TENG as shown. As described above, it is assembled so that current can be generated through repetition of press and release. To investigate the electrical output performance of the transparent TENG, the detailed electrical characteristics of the device were checked. During periodic stress by a linear mechanical motor at a specific frequency (6 Hz), the open voltage and short-circuit current of a typical TENG device with a size of 3 cm × 3 cm reach up to 40 V and 35 nA (each corresponding to a current density of 320 nA cm-2, respectively). This result is almost 100 times higher than non-MQD coated TENG. This increase in voltage can be seen as a result of strengthening the electrostatic phenomenon by increasing the effect of the negative layer by MQD (MXene quantum dot). As shown in Figure 18, MXene is a highly negatively charged material, and it appears to maximize the triboelectric effect by forming a thin negative layer while maintaining the pattern structure on the patterned PDMS in the form of quantum dots. The current density increase of the MQD coated ZnO-PET TENG identified in Figure 17 can be explained by UPS analysis (Fig. 19). As shown in Figure 20, we were able to calculate the conduction band (CB), valence band (VB), and band gap of ZnO and MQD through the UPS graph. ZnO and MQD have a band gap of 3.3 eV and 2.8 eV, respectively, which is confirmed to cause an increase in current density by allowing the MQD to have a band gap lower than ZnO to easily transfer electrons to ZnO at the outermost surface of the electrode.

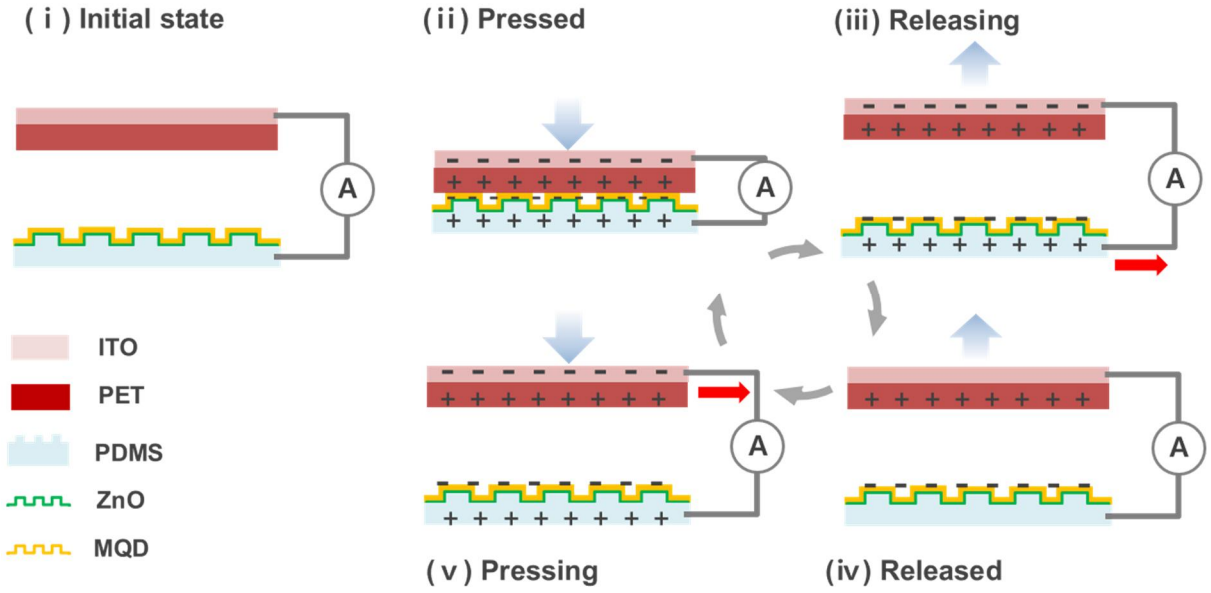

Figure 15. The schematic diagram of the TENG

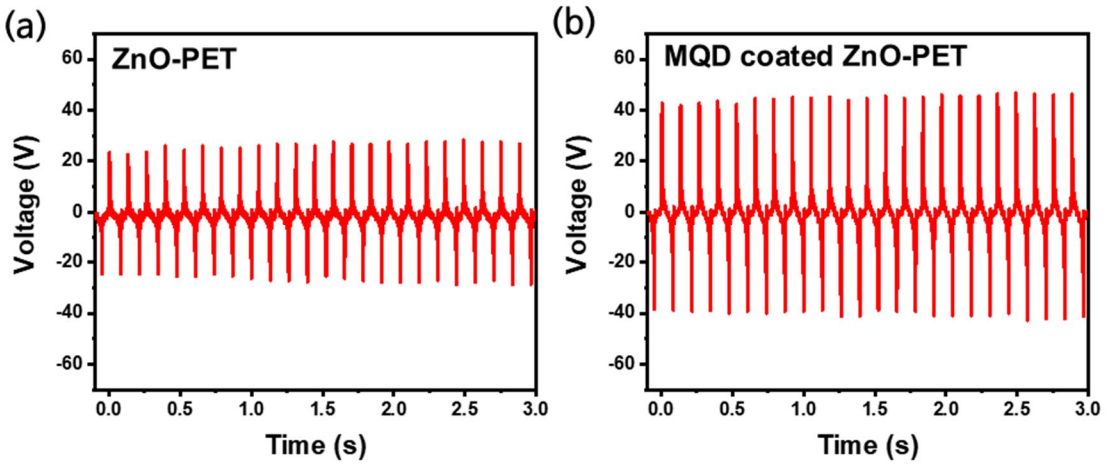

Figure 16. The open-circuit voltage (Voc) at a 6 Hz (a) ZnO-PET, (b) MQD coated ZnO-PET

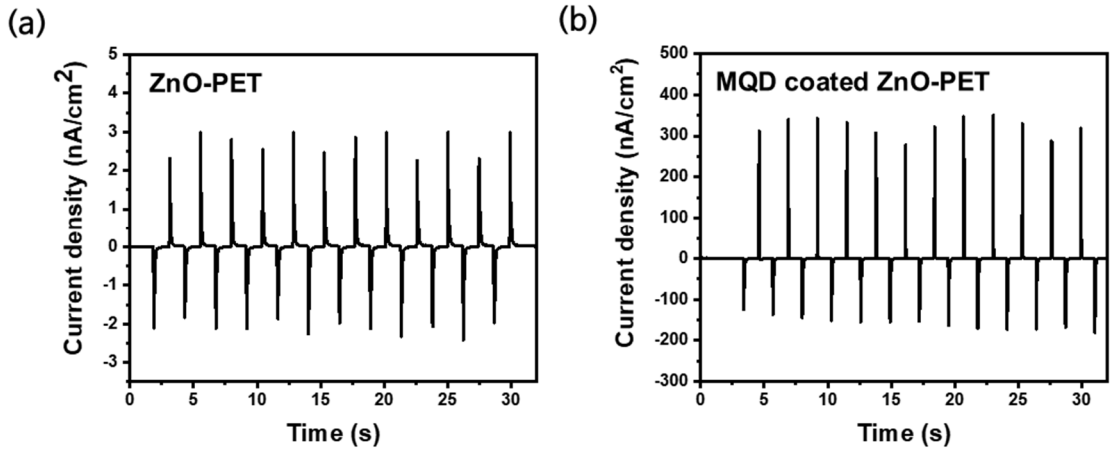

Figure 17. Short-circuit current density of a TENG (a) ZnO- PET, (b) MQD coated ZnO-PET

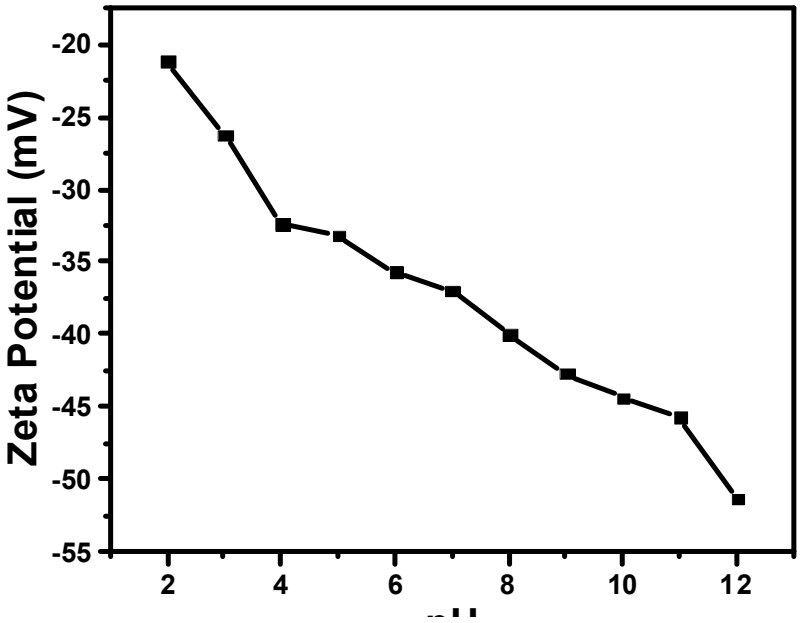

Figure 18. Zeta potential of MXene solution

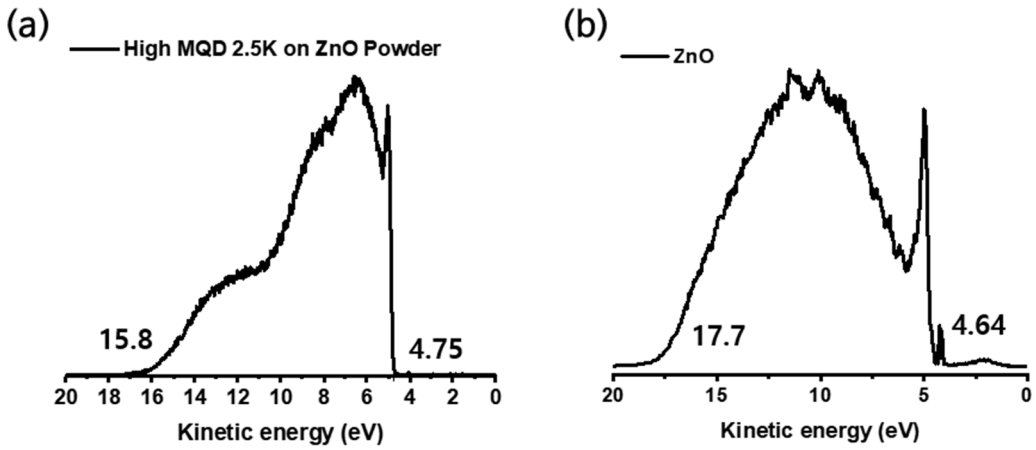

Figure 19. UPS of MQD on ZnO and ZnO

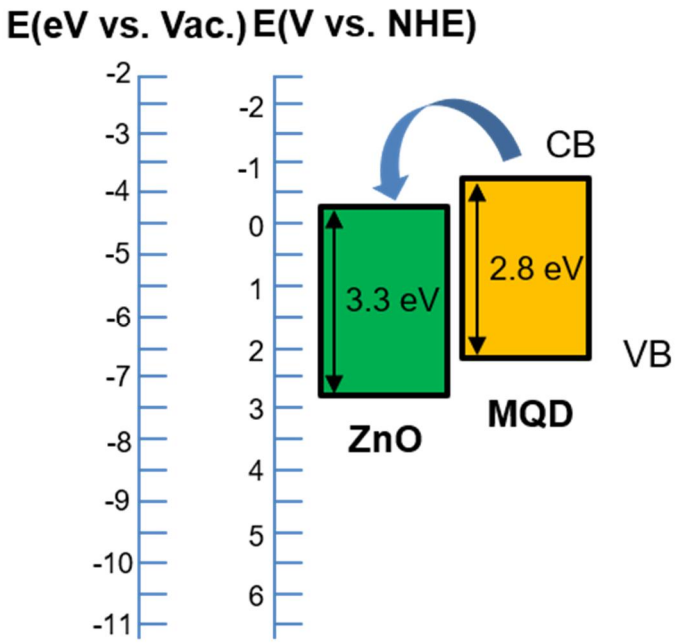

Figure 20. Calculated band gap of MQD and ZnO

2.3 Conclusion

In this study, for higher output of TENG, MXene quantum dots were applied to the electrodes when operating as active materials to make the electrodes more negatively charged. PEIs of various molecular weights were used for the synthesis of MQDs, and MQDs synthesized with PEIs with a molecular weight of 25k showed the best performance. The negatively charged MQD strengthened the triboelectric effect at the electrode surface, resulting in a 40V output that was twice the value of bare ZnO. In addition, MQD has a band gap of 2.8 eV, which is lower than the band gap of ZnO, 3.3 eV, and effectively serves to transfer electrons generated by the triboelectric effect to the electrode on the surface of ZnO. As a result, an electrode material having a value of 300 nA/cm^2, which is a current density of about 100 times that of the conventional one, has been successfully synthesized.

Reference

1. Sebald, G.; Guyomar, D.; Agbossou, A., On thermoelectric and pyroelectric energy harvesting. *Smart Materials and Structures* **2009,** *18* (12).

2. Ru Ng, A. Y.; Boruah, B.; Chin, K. F.; Modak, J. M.; Soo, H. S., Photoelectrochemical Cells for Artificial Photosynthesis: Alternatives to Water Oxidation. *ChemNanoMat* **2020,** *6* (2), 185-203.

3. Huang, L.-b.; Xu, W.; Bai, G.; Wong, M.-C.; Yang, Z.; Hao, J., Wind energy and blue energy harvesting based on magnetic-assisted noncontact triboelectric nanogenerator. *Nano Energy* **2016,** *30*, 36-42.

4. Barkas, D. A.; Psomopoulos, C. S.; Papageorgas, P. M.; Kalkanis, K.; Piromalis, D.; Mouratidis, A., Sustainable Energya Harvesting through Triboelectric Nano – Generators: A Review of current status and applications. *Energy Procedia* **2019,** *157*, 999-1010.

5. Fan, F.-R.; Tian, Z.-Q.; Lin Wang, Z., Flexible triboelectric generator. *Nano Energy* **2012,** *1* (2), 328-334.

6. Hinchet, R.; Seung, W.; Kim, S. W., Recent Progress on Flexible Triboelectric Nanogenerators for SelfPowered Electronics. *ChemSusChem* **2015,** *8* (14), 2327-44.

7. Kim, Y. J.; Lee, J.; Park, S.; Park, C.; Park, C.; Choi, H.-J., Effect of the relative permittivity of oxides on the performance of triboelectric nanogenerators. *RSC Adv.* **2017,** *7* (78), 49368-49373.

8. Lee, J. P.; Lee, J. W.; Baik, J. M., The Progress of PVDF as a Functional Material for Triboelectric Nanogenerators and Self-Powered Sensors. *Micromachines (Basel)* **2018,** *9* (10).

9. Li, D.; Wu, C.; Ruan, L.; Wang, J.; Qiu, Z.; Wang, K.; Liu, Y.; Zhang, Y.; Guo, T.; Lin, J.; Kim, T. W., Electron-transfer mechanisms for confirmation of contact-electrification in ZnO/polyimide-based triboelectric nanogenerators. *Nano Energy* **2020,** *75*.

10. Wu, C.; Wang, A. C.; Ding, W.; Guo, H.; Wang, Z. L., Triboelectric Nanogenerator: A Foundation of the Energy for the New Era. *Advanced Energy Materials* **2019,** *9* (1).

11. Zhang, C.; Ma, Y.; Zhang, X.; Abdolhosseinzadeh, S.; Sheng, H.; Lan, W.; Pakdel, A.; Heier, J.; Nüesch, F., Two□Dimensional Transition Metal Carbides and Nitrides (MXenes): Synthesis, Properties, and Electrochemical Energy Storage Applications. *Energy & Environmental Materials* **2020,** *3* (1), 29-55.

12. Alhabeb, M.; Maleski, K.; Anasori, B.; Lelyukh, P.; Clark, L.; Sin, S.; Gogotsi, Y., Guidelines for Synthesis and Processing of Two-Dimensional Titanium Carbide (Ti3C2Tx MXene). *Chemistry of Materials* **2017,** *29* (18), 7633-7644.

13. Sarycheva, A.; Polemi, A.; Liu, Y.; Dandekar, K.; Anasori, B.; Gogotsi, Y., 2D titanium carbide (MXene) for wireless communication. *SCIENCE ADVANCES* **2018,** *4* (9), eaau0920.

14. Xu, Y.; Liu, J.; Gao, C.; Wang, E., Applications of carbon quantum dots in electrochemiluminescence: A mini review. *Electrochemistry Communications* **2014,** *48*, 151-154.

15. Kim, S. J.; Koh, H. J.; Ren, C. E.; Kwon, O.; Maleski, K.; Cho, S. Y.; Anasori, B.; Kim, C. K.; Choi, Y. K.; Kim, J.; Gogotsi, Y.; Jung, H. T., Metallic Ti3C2Tx MXene Gas Sensors with Ultrahigh Signal-to-Noise Ratio. *Acs Nano* **2018,** *12* (2), 986-993.